eprints@whiterose.ac.uk
https://eprints.whiterose.ac.uk/

Landslides induced by the 2010 Chile megathrust earthquake: a comprehensive inventory and correlations with geological and seismic factors

Alejandra Serey [(1)], Laura Piñero-Feliciangeli[(2)] , Sergio A. Sepúlveda [(1,2)], Fernando Poblete [(2)], David N. Petley [(3)], William Murphy [(4)]

    (1) Departamento de Geología, Universidad de Chile, alejandra.serey@gmail.com
    (2) Instituto de Ciencias de la Ingeniería, Universidad de O´Higgins.
    (3) Department of Geography, University of Sheffield.
    (4) School of Earth and Environment, University of Leeds.

ABSTRACT (150-250 words)

The 2010 Mw=8.8 Maule earthquake, which occurred in the subduction contact between the Nazca and the South American tectonic plates off the coast of Chile, represents an important opportunity to improve understanding of the distribution and controls for the generation of landslides triggered by large megathrust earthquakes in subduction zones. This paper provides the analysis of the comprehensive landslide inventory for the Maule earthquake between 32.5° S and 38.5° S°. In total 1226 landslides were mapped over a total area of c.120,500 km^2 , dominantly disrupted slides. The total landslide volume is c. 10.6 Mm^3. The events are unevenly distributed in the study area, the majority of landslides located in the Principal Andean Cordillera and a very constrained region near the coast on the Arauco Peninsula, forming landslide clusters. Statistical analysis of our database suggests that relief and lithology are the main geological factors controlling coseismic landslides, while the seismic factor with higher correlation with landslide occurrence is the ratio between peak horizontal and peak vertical ground accelerations. The results and comparison with other seismic events elsewhere suggest that the number of landslides generated by megathrust earthquakes is lower than events triggered by shallow crustal earthquakes by at least one or two orders of magnitude, which is very important to consider in future seismic landslide hazard analysis.

Keywords: coseismic landslides, megathrust earthquake, Chile.

INTRODUCTION

Landslides represent perhaps the most frequent geological hazard present in mountainous environments, due to the geological, geomorphological and geotechnical characteristics of steep upland landscapes. Most notably, in tectonically-active mountain areas, landslides are a major cause of fatalities and economic losses during and after strong earthquakes (e.g. Sepúlveda et al. 2005; Jibson et al. 2006; Sato et al. 2007; Qi et al. 2010; Dai et al. 2011).

A key focus for research on seismically-triggered landslides in high mountain areas had been the development of approaches to create reliable estimates of the likely pattern of landslides in future earthquakes. This has usually undertaken through the development of statistical relations between specific earthquake events of different magnitudes and the number, area or volume of landslides triggered by each event (e.g. Keefer 1984, Rodriguez et al. 1999, Malamud et al. 2004a, Malamud et al. 2004b, Marc et al. 2016, Havenith et al. 2016). Recently Marc et al. (2016) compiled and analysed extensive databases of over 40 earthquakes ranging between Mw=5.1 and Mw=8.6, with a primary focus on shallow crustal earthquakes, allowing the presentation of a seismologically consistent expression for the total area and volume of populations of earthquake-triggered landslides. Similarly, Malamud et al (2004a), provided quantitative estimates of the total number of landslides (N_{LT}) expected for an earthquake of a given magnitude; for example this estimates that around 500,000 landslides would be generated for an event om the scale of the 2010 Mw=8.8 Maule earthquake, which occurred in the subduction zone between the Nazca and the South American tectonic plates of the coast of Chile. However, in comparison with shallow crustal earthquakes the number of complete landslide inventories for subduction zone earthquakes is small, meaning that there is huge uncertainty in such estimates. Prior to the study reported here, only one fully comprehensive, reliable inventory of coseismic landslides, based on field inventories and visual analysis of aerial or satellite images, has been available for subduction zone earthquakes. This is the inventory for the 2011 Mw=9.0 Tohoku earthquake (Wartman et al. 2013). Therefore, there is a

need to improve these datasets. The 2010 Maule earthquake, reported here, provides a key opportunity to understand better the distribution and controls for the generation of landslides triggered by large subduction zone earthquakes.

This paper builds on the pilot study of Serey et al. (2017) to provide a comprehensive inventory of landslides induced by the Maule earthquake, and to analyse their correlations with geological (slope, lithology) and seismic factors (rupture distance, PGA, PGV), thereby providing new insight into the factors controlling coseismic landslides in subduction zone earthquakes.

THE 2010 Mw=8.8 MAULE EARTHQUAKE

The 2010 Mw=8.8 Maule earthquake, which occurred on 27 February 2010, is the sixth largest event in the United States Geological Survey (USGS) global catalogue and the second largest to have been recorded in Chile, just behind the 1960 Valdivia earthquake. It is the largest earthquake to have been recorded instrumentally in Chile. The rupture zone matches a seismic gap dating to 1835. Prior to the earthquake, several authors (Campos et al., 2002, Moreno et al. 2008, Ruegg et al., 2009), suggested that the area had a high probability of generating an earthquake in the near future, based on GPS data that showed an eastward terrain shift up to 4 cm a^{-1} (Cisternas 2011).

The earthquake rupture was located along the tectonic zone in which the Nazca plate is subducted beneath the South American plate, for which the convergence rate is c.6.6 cm a^{-1} (Angermann et al., 1999). The hypocenter was located at the geographic coordinates 36.290° S, 73.239° W with a depth of 37 km according to the National Seismological Service of University of Chile (SSN). The rupture zone extended 450 km along the Chilean coast and 150 km from east to west. The speed and time of propagation is of the order of 2.5 to 3.5 km / s and 110 s respectively (Barrientos 2010).

Thirty-two accelerometers recorded the strong motion, with reliable peak values of 0.93 g (horizontal component) at Angol station and 0.70 g (vertical component) at Llolleo station (Boroschek et al., 2012; Figure 1).

The rupture process of the Maule earthquake was characterized by the behaviour of asperities (Lay et al. 2010, Delouis et al., 2010, Tong et al., 2010, Lorito et al., 2011) (Figure 1). An asperity with high levels of slip (the main asperity) was located in the northern part of the seismic gap, approximately in the same rupture area as the 1928 Mw=7.6 Talca earthquake (Ruiz et al., 2012).
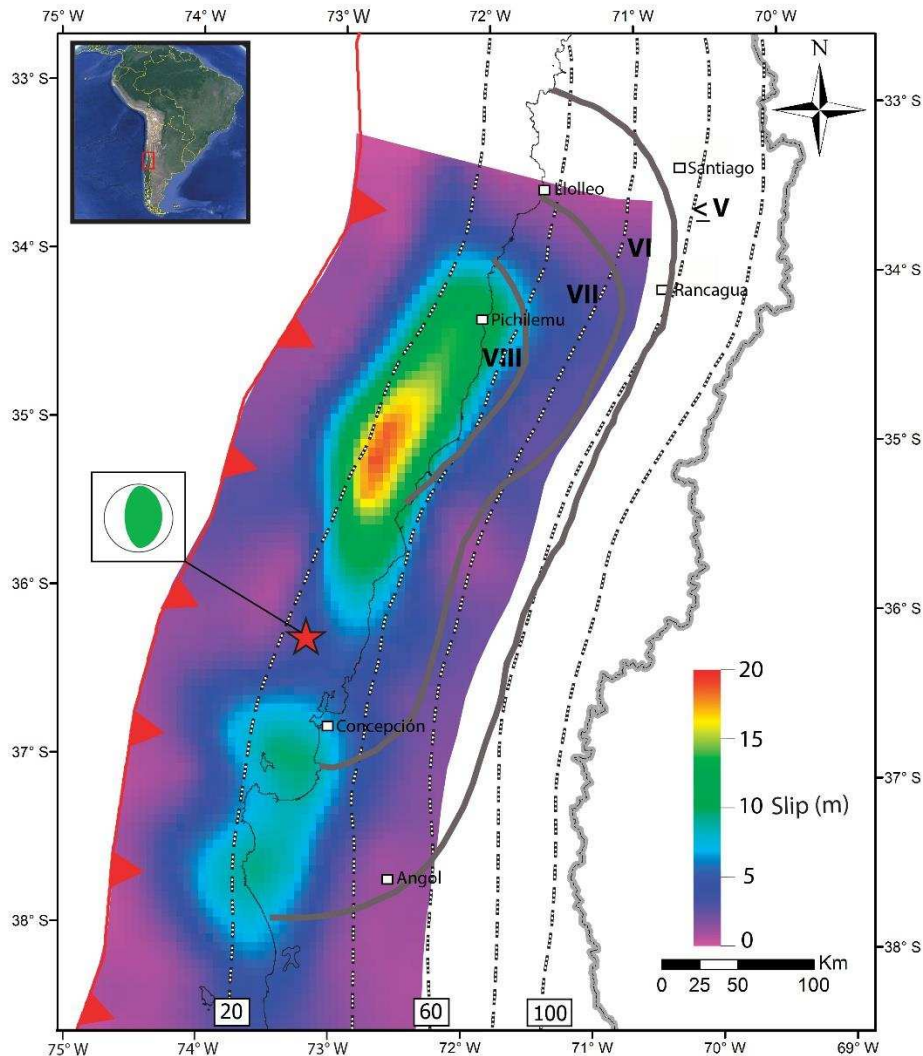
Figure 1. Rupture zone, slip distribution (extracted from Lorito et al. 2013) and the isoseismal map (grey lines) inside the damage area of 2010 Maule earthquake (based upon data from Astroza et al. 2012). The red line with triangles is the trench between the Nazca and South America Plates (Bird, 2003), Slab1.0 plate interface contours from the USGS (grey dotted lines). The green and white focal mechanism is taken from the United States Geological Survey centroid moment tensor.

GEOLOGICAL AND GEOMORPHOLOGICAL SETTING OF THE COSEISMIC LANDSLIDES

The Andes represent the geodynamic archetype of a convergent, non-collisional mountain range, generated by subduction of the oceanic lithosphere of the Nazca (Farallon) Plate beneath the continental lithosphere of the South American Plate (Pardo-Casas and Molnar, 1987). Consequently, the present-day architecture of the Andes Mountains is largely the result of convergence between the Pacific–Nazca and South American plates. These mountains are a consequence of crustal shortening, principally accommodated by eastward thrusting, which leads to crustal thickening and surface uplift (Isacks 1988; Sheffels 1990; Allmendinger et al. 1997). Subduction is also evidenced by an almost continuous line of both active and dormant volcanoes, mostly andesitic stratovolcanoes, which run almost the entire length of the country. The Andes of Central Chile (32.5° S to 41.5° S) are composed of a number of morphostructural units from west to east: the Coastal Cordillera, the Central Valley, the Principal Cordillera (spanning Chile and Argentina), the Frontal Cordillera, the Argentine Precordillera and the Pampean Ranges (Jordan et al. 1983). For reference, Figure 2 shows a simplified geologic map and the distribution of slope angle in the area of the Maule earthquake coseismic landslide inventory (elevation

data for the slope angle map is coming from ASTER GDEM, product of METI and NASA, resolution 30 m). The Chilean Coastal Cordillera consists of low and topographically-smooth mountains composed predominantly of Late Paleozoic and Mesozoic igneous rocks, with paired belts of Paleozoic metamorphic rocks cropping out south of Pichilemu (34º S). The Central Valley is a depression with a Mesozoic to Quaternary sedimentary infill (Charrier et al. 2015; Pankhurst and Hervé 2007); from Santiago to the south, this is the main agricultural zone and contains several major cities, including the capital. The Principal Cordillera is a chain of high mountains with a strong relief and steep slopes that in its western part in Chilean territory mostly comprises Oligocene–Miocene continental volcaniclastic rocks, intruded by Miocene–Pliocene granitoids (Charrier et al. 2015; Pankhurst and Hervé 2007). The Frontal Cordillera is composed of units formed during the Gondwana orogeny in the Late Palaeozoic to Early Mesozoic. Older Palaeozoic rocks appear in the Pampean range.
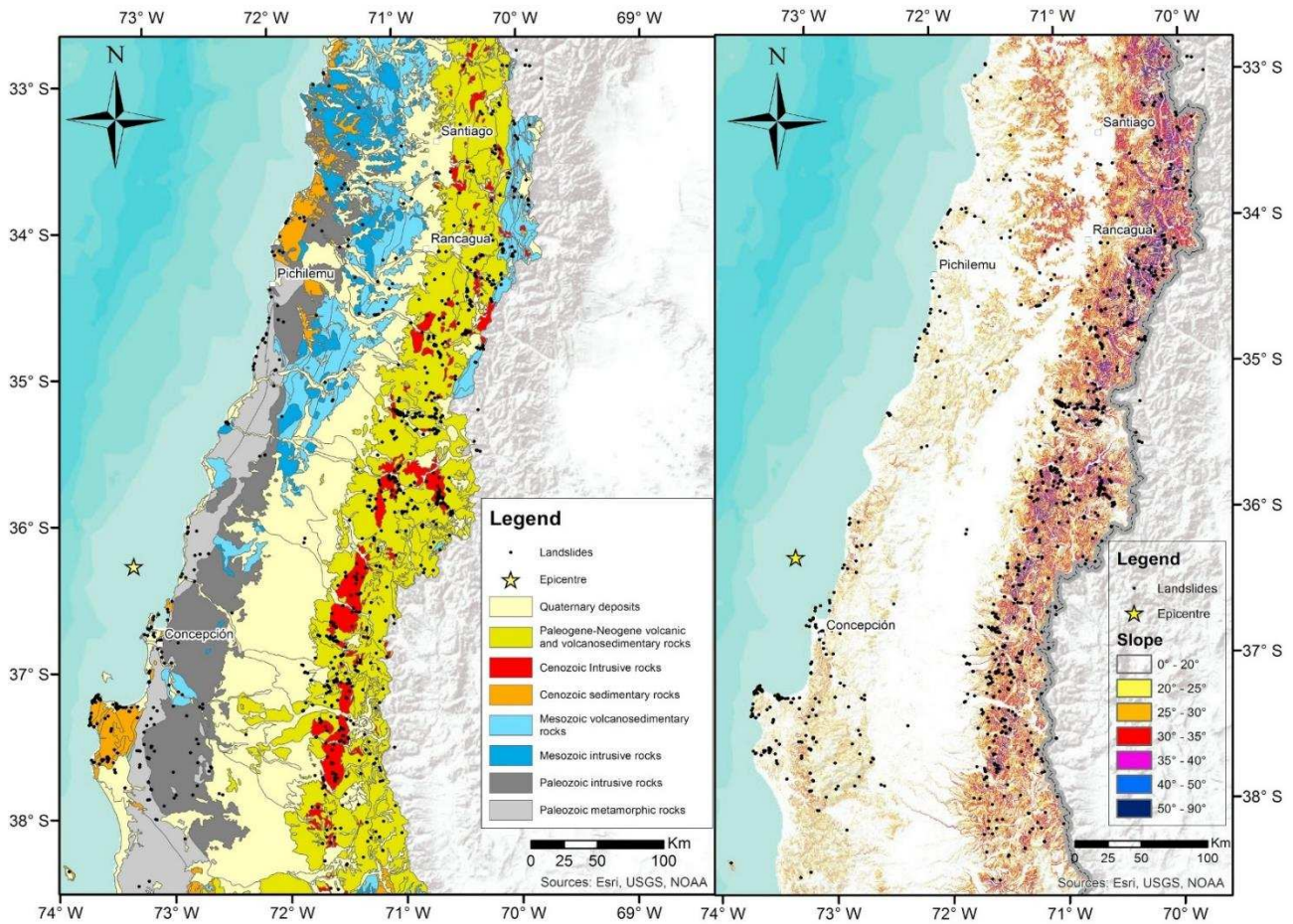

Figure 2. Simplified geologic map (modified from SERNAGEOMIN, 2003) and the distribution of slope angle in the area of 2010 coseismic landslide inventory.

THE 2010 Mw=8.8 MAULE EARTHQUAKE GROUND MOTION DISTRIBUTION

Interpolated maps of the peak horizontal and vertical acceleration components (PGAH), (PGAV) and normalized PGAH/PGAV values have been generated (Figure 3), based on information available from 32 stations from the strong motion network of the National Seismological Centre, Universidad de Chile (see supplementary material (S1) for detailed information). The interpolation methodology used for all maps was based on an adjustable tension continuous curvature surface gridding algorithm, with the tension parameter set to 0.25. The implementation was done using Generic Mapping Tools (GMT).

In previous studies co-seismic landslide initiation has in general been related to the peak horizontal ground acceleration parameter (PGAH) (following Terzaghi, 1950). For the Maule earthquake the

maximum horizontal acceleration recorded was 1.25 g at Cauquenes station, although the accelerometer saturated because the different components over-crossed (Saragoni & Ruiz, 2012). Thus the PGAH value for Cauquenes has not been included in our analysis (Figure 3a) because it is not considered to be a reliable measurement.

The distribution of PGAH values of the 2010 Mw=8.8 Maule Earthquake show a minimum measured ground shaking value of 0.02 g at Vallenar station (latitude -28.576) north of the study area, and a maximum reliable value at Angol station of 0.97 g. However, Angol may have been severely affected by site effects (Felipe Leyton, personal communication), which directly affects the interpolation result, indicating a zone of intense shaking centered at Angol. In general, the Tohoku 2011 Earthquake generated higher values of PGAH (max. = 2.02 g) (Wartman et al., 2013) than the Maule Earthquake.

In common with Saragoni & Ruiz (2012), our PGAH map shows attenuation towards the east, with peak PGAH values reducing from c.1.0 g to c.0.2 g for distances of 100 km from the rupture plane that defines the main asperity.

The PGAV distribution is shown in Figure 3b (see supplementary data (S1) for detailed information). The recorded values for this parameter range between 0.008 and 0.700 g. Notably, the spatial distribution of PGAV does not resemble the PGAH map. From Figure 3b, a peak value of 0.7 g at Llolleo in the north of the rupture area, and a more extended area of high values (up to 0.55 g) recorded near the coast at Concepcion close to the southernmost asperity, dominate the pattern. PGAV values are typically c.0.3 g at a distance of 100 - 120 km from the asperities.

In Figure 3c we show the ratio between PGAH and PGAV. An interesting pattern is observed for this parameter, giving smaller values near the coast, nearer to the asperity, and greater values are observed in further regions, up to 120 - 140 km from the asperities at the Principal Cordillera.
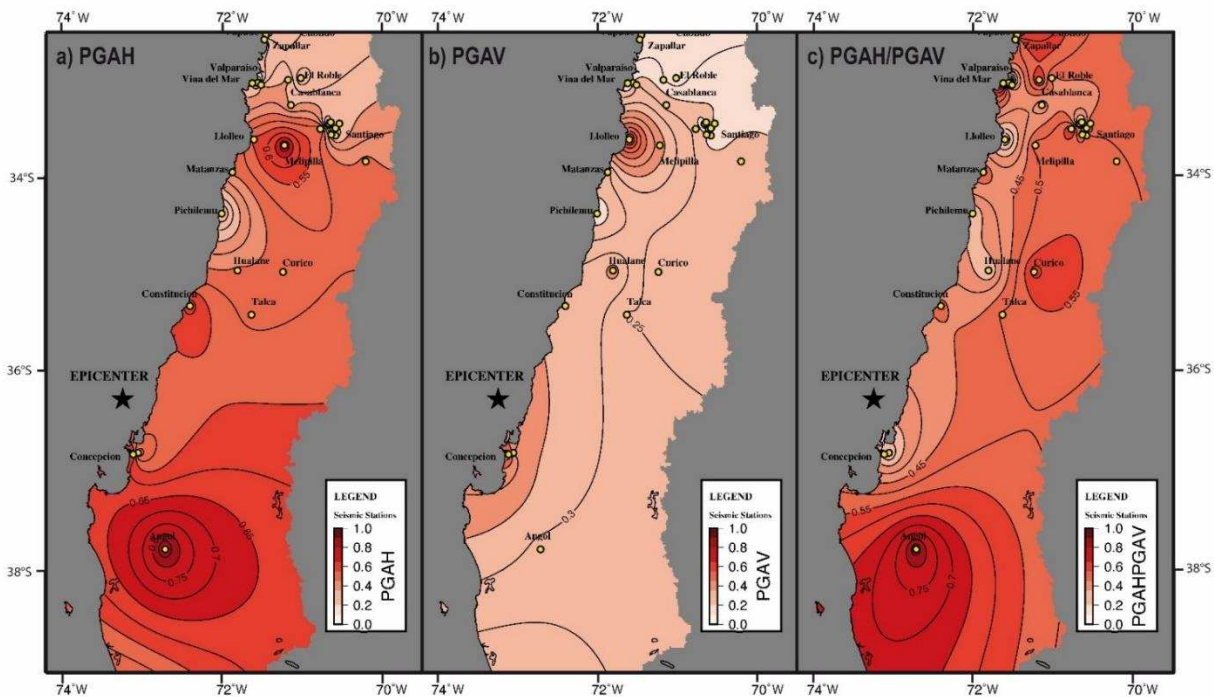

Figure 3. Interpolated maps of the peak ground accelerations of a) PGAH, b) PGAV and c) PGAH/PGAV ratio obtained from 32 stations from the Accelerograph Chilean Network from Universidad de Chile.

LANDSLIDES INDUCED BY THE 2010 MAULE MEGATHRUST EARTHQUAKE

Landslide inventory and correlations with relief and geology

Serey et al. (2017) presented a pilot inventory of landslides generated by the Maule earthquake from the analysis of satellite images and bibliographic information for a part of the area affected by the earthquake, between 32.5° S and 38.5° S°, with the Chile-Argentina border providing the eastern boundary of the mapped area. This paper expands the dataset to the Principal Cordillera (Argentine side) and the Frontal Cordillera, providing for the first time a complete landslide inventory for the Maule earthquake. This represents only the second full inventory of coseismic landslides for a subduction zone earthquake based on field inventories and visual analysis of aerial or satellite images.

For the bibliographic compilation, Serey et al. (2017) collected information about recorded landslides events triggered by the Maule earthquake. They reviewed 107 technical reports of the National Geological and Mining Survey of Chile (SERNAGEOMIN) related to the earthquake, from which the relevant information pertaining to landslides and lateral spreads was extracted. They also reviewed the georeferenced reports of road network interruption problems caused by the earthquake, undertaken by the Ministry of Public Works and incorporated an inventory of lateral spreads provided by Verdugo et al. (2012), and the inventory of landslides in the coastal fringe of the Biobio administrative region provided by Mardones and Rojas (2012).

The landslides were mapped by interpreting Landsat satellite images (Landsat 5-7-8, Provider:NASA, resolution: 30 m, mostly temporal span: 2008-2013) before and after the earthquake using Google Earth. A visual inspection of these strips was done at an eye height of ~1-2 km, decreasing the height when an alteration was detected in the vegetation, or when bare spots or typical mass movement morphologies were present (Soeters and Van Western 1996). We visually inspected the earliest available images after the earthquake, mapping at 1:2000 and 1:10,000. Once a landslide was identified, the location was compared with the latest available pre-seismic image without cloud or snow cover and the landslide was mapped as polygon. Validation fieldwork was undertaken in the coastal regions, where the higher densities of landslides are located, in order to identify and classify landslides by failure mode. Field inspections allowed the addition of a number of small mass movements that were not identified in the satellite images. The minimum size considered for the mapping was 30 m^2, although field inspections showed that an indefinite number of small mass movements were not recognized on the satellite images. Thus in keeping with all such studies, our inventory is censored for very small landslides (i.e. those with a surface area of less than 30 m^2).

In total 1226 landslides were mapped (Figure 4) over a total area of c.120,500 km^2. The maximum distance to the epicentre is 487 km. The total landslide volume is c. 10.6 Mm^3, estimated using published area-volume relationships proposed by Larsen et al. (2010) (Methodology is described in supplementary material S1). The inventory includes 1059 disrupted slides, 110 flows, 49 lateral spreads and eight coherent slides, following the Keefer (1984) classification for earthquake-induced landslides. Most of the landslides (over 850, mainly disrupted shallow slides and falls) are located in the farther Andes Principal Cordillera, which has a stronger relief and steeper slopes than the Coastal Cordillera, despite the lower earthquake intensities. A large number of landslides (387) are in the size range of 1000 m^2 to 5000 m^2, while just a few (29) have more than 50,000 m^2. Landslides located in the Central Valley are limited and are mainly lateral spreads caused by liquefaction.

The compiled dataset has been compared with the curves by Keefer (1984) and Rodriguez et al. (1999) regarding the maximum landslide area and the epicentral distance (Serey et al., 2017). It was observed that the geographical distribution is in agreement with the predictions defined for an earthquake of magnitude Mw=8.8. However, the events are not evenly distributed in the study area, and Serey et al. (2017) highlighted the presence of landslide clusters. The most important cluster (127 failures) is located in the Arauco Peninsula, Biobio region, mainly triggered in low strength Neogene, marine sedimentary rocks. These rocks has been tested by Moya (2016), showing differential stress-strain behaviour depending on the testing conditions and an increase in the shear strength under cyclic testing.
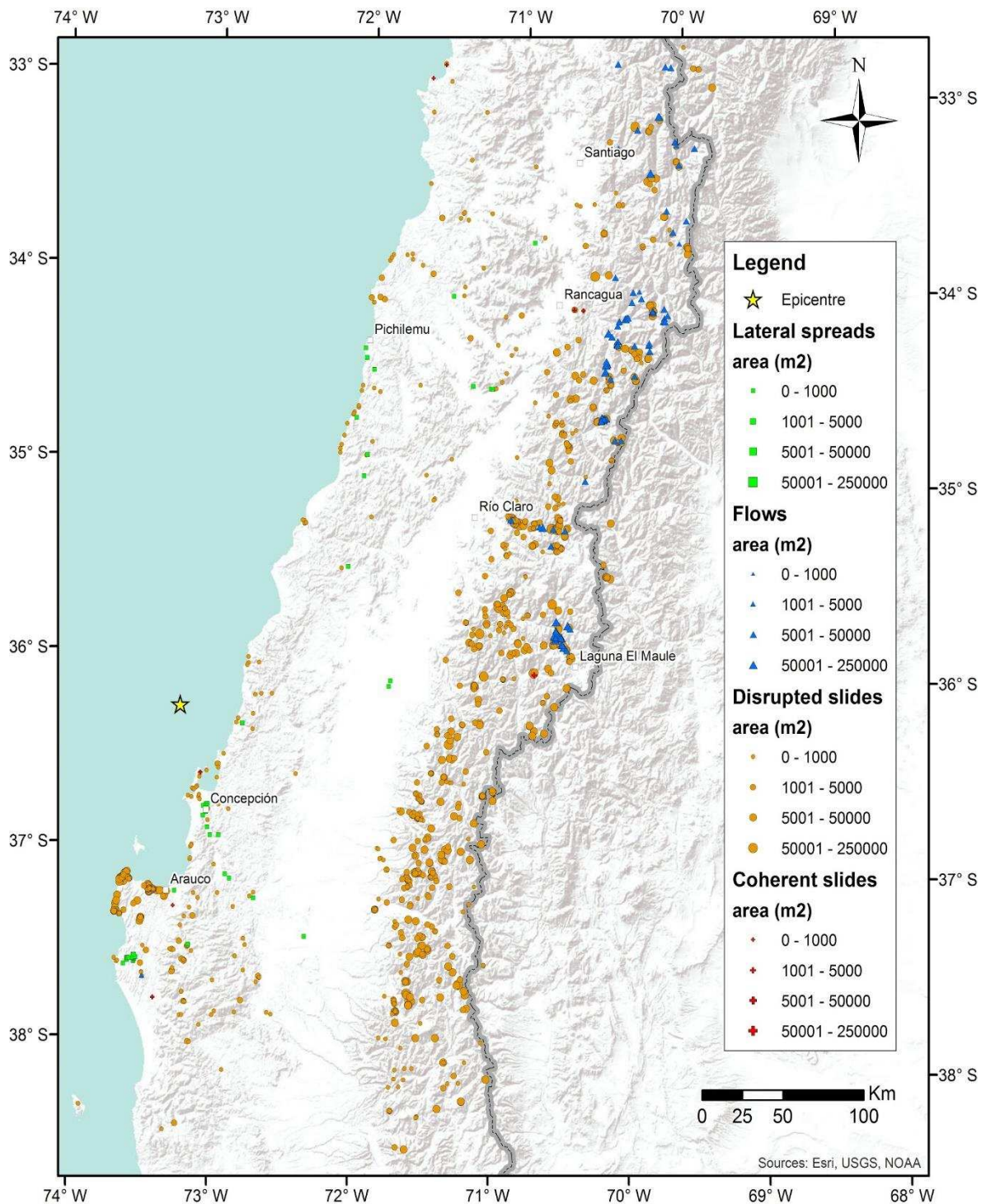
Figure 4. The comprehensive landslide inventory for the 2010 Maule earthquake.

Figure 5a shows a 3D histogram of landslide counts normalized by geologic unit area based on the landslide classification, simplified geologic units and landslides types. Landslide occurrence is more frequent in Paleogene-Neogene volcanic and volcano sedimentary rocks, with a total of 42% of landslides. The Quaternary deposits and Cenozoic intrusive rocks represent 20% and 16 %, respectively. In total, these three geologic units cover 79 % of the whole inventory. Disrupted landslides were the dominant type of landslides triggered by the 2010 Maule earthquake. Other types of landslides, coherent

slides and flows and lateral spreads were minor, representing less than 2% of the total. The percentage of disrupted landslides generated in Paleogene-Neogene volcanic and volcano sedimentary rocks, which was the most dominant from the classified geologic units, covered c.41%. The other two most important geological units that exhibit landslide occurrence were Quaternary deposits and Cenozoic intrusive rocks, adding up 36 % of the total. In other words, the majority of the landslides triggered by the Maule earthquake occurred in the youngest geological units in the area. Furthermore, in one of the landslide clusters of the Maule inventory, in the Arauco Peninsula, landslides were mainly triggered in low strength Neogene, marine sedimentary rocks, suggesting an important lithologic control as a major factor in the generation of landslides (Moya et al., 2015; Moya, 2016). These results coincide well with those obtained for coseismic landslides triggered by the 2011 Tohoku earthquake (Mw=9.0, subduction earthquake), where majority of landslides occurred in the youngest (Neogene) geologic units of the region (Wartman et. al 2013). Thus, for both comprehensive megathrust coseismic landslide inventories lithology proves to be an extremely important factor.

In total, 55% of landslides occurred on slope angles between 20º and 40º (Fig 5b), whilst 39% of landslides occurred between on slopes of less than 20º. In contrast, less than 6.3 % of slope failures occurred for angles greater than 40º. This predominance of coseismic landslides on slopes between 20° and 40° has been observed elsewhere, including the 2005 Mw=7.6 Kashmir earthquake (Sato et al 2007, Kamp et al 2008, Owen et al 2008) and the 2008 Mw=8.3 Wenchuan earthquake (Gorum et al. 2011).

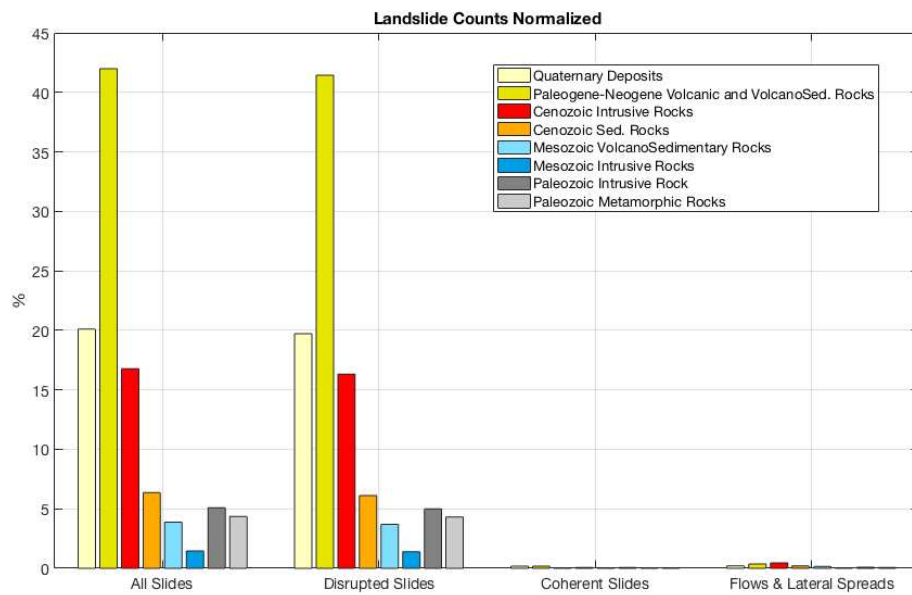**Spatial analysis of coseismic landslide distribution and ground motion**
The spatial pattern of landslides was analysed calculating a map of landslide density or landslide concentration (LC). The calculation was done across a moving grid of size 0.5º x 0.5º through the 120,500 km^2 landslide-affected area. LC was defined as:

LC = (Sum area of all landslides within the grid)/(total area of the grid).

Python and GMT (Generic Mapping Tool) scripting were used for the implementation of the calculation.

In Figure 6 the LC results from calculation is shown for: a) all landslides, b) coherent slides, c) disrupted slides and d) flows and lateral spreads triggered by the 2010 Mw=8.8 Maule earthquake. The LC map for all landslides (Figure 6a) shows that the events are very unevenly distributed in the study area, with the majority of landslides are located in the Principal Andean Cordillera (especially in the vicinity of Río Claro, Laguna El Maule, Rancagua) and a limited zone near the coast on the Arauco Peninsula, as noted previously.
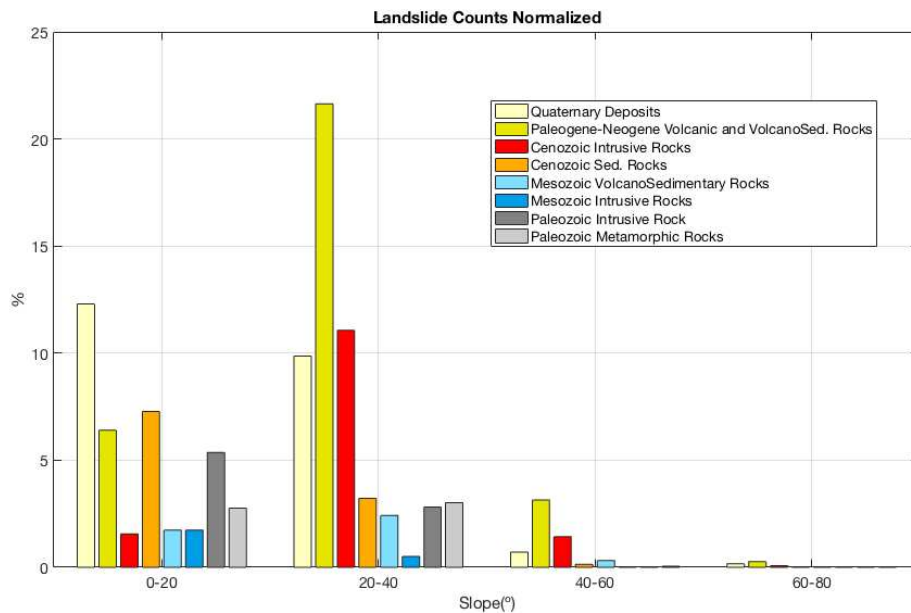
a)

b)

Figure 5. 5a) Histogram of landslide counts normalized by geologic unit based on landslide classification, simplified geologic units and landslides types. 5b) histogram shows, landslides counts normalized by geologic units and disaggregated slope intervals of 20º.

Coherent slides provide less than 0.5% of the whole database and are well constrained in the Laguna El Maule cluster (Figure 6b). The geologic units with maximum coherent landslide occurrence are the Quaternary deposits and Paleogene-Neogene volcanic and volcano-sedimentary rocks.

Disrupted landslides were concentrated in two main areas, corresponding to the Rio Claro and Arauco clusters noted above (Figure 6c). The Rio Claro cluster, with an approximate area of 2,500 km^2, lies in

an area in which Paleogene-Neogene volcanic and volcanic sedimentary rocks, in which Cenozoic intrusive rocks crop out. The second disrupted slides cluster lies near the coast in the Arauco zone, with an area of c.500 km^2, where Cenozoic sedimentary rocks are the main geologic unit cropping out in the area. The areas of high concentration for flows and lateral spreads, which represent less than 2% of the total, correspond to the Laguna El Maule and Rancagua clusters (Figure 6d).
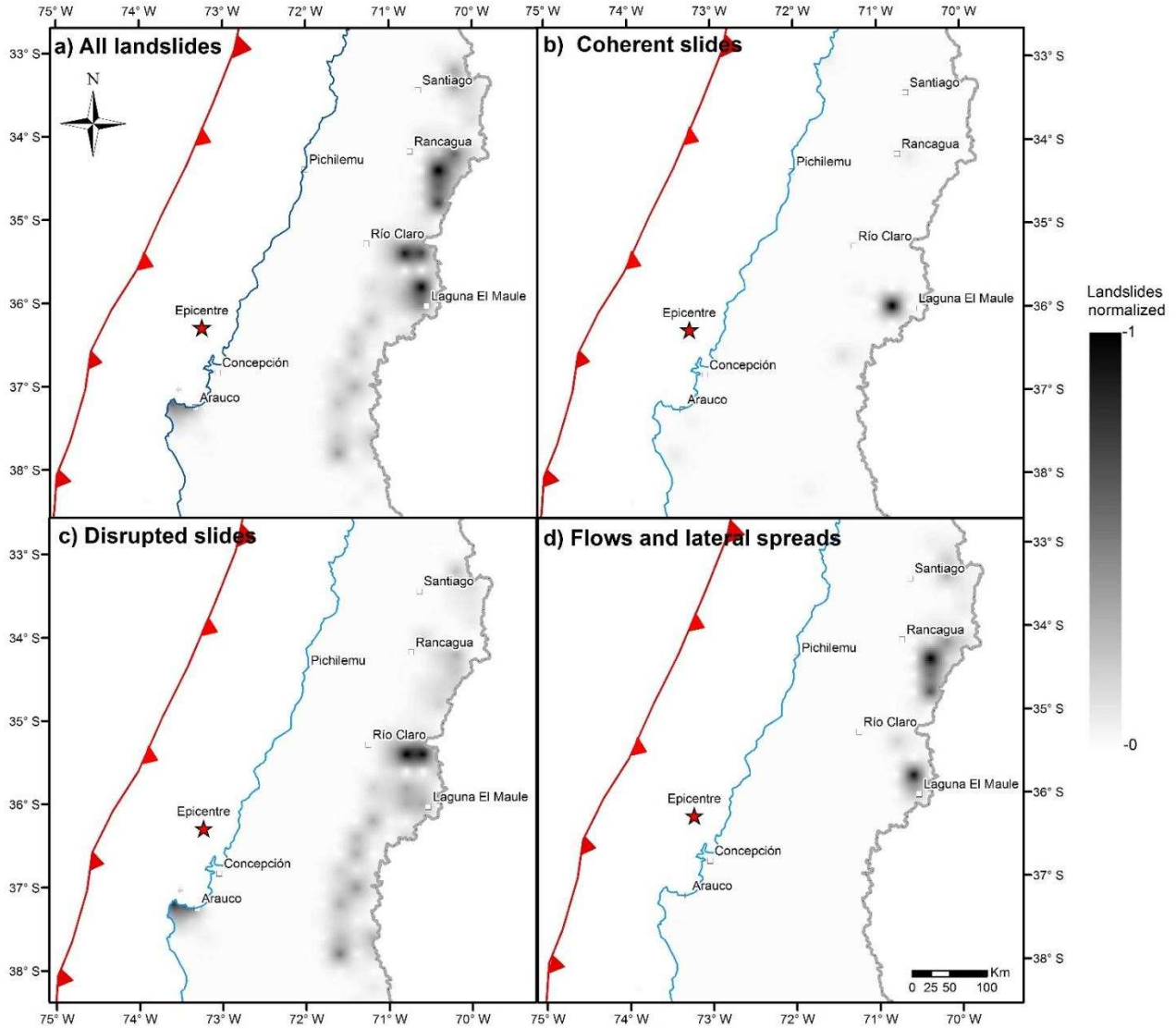

Figure 6. Landslide concentrations (LC) normalized to the maximum concentration value. Areas in dark colours shows landslides clusters described in the text. In blue coastline. The red line with triangles is the trench between the Nazca and South America Plates (Bird, 2003). a) LC of all landslides. b) LC of coherent slides. c) LC of disrupted slides. d) LC of flows and lateral spreads.

The spatial distribution of PGAH has two zones of higher shaking, with the largest being located at Angol in the south of our study area and the other in the area of Melipilla in the north, near Santiago. There is no evident correlation between the horizontal peak ground acceleration and the LC distributions for different landslides types (disrupted slide, coherent, flows and lateral spreads). It is noted that the PGAV the values attenuate from west to east from Concepcion (maximum value of 0.55 g) to smaller values in the east of the country. This means that for the locations of high landslide concentration the values for the vertical acceleration parameter are low, typically less than 0.3 g. In conclusion, our analysis suggest no evident correlation between the LC distribution and the regional

PGA distribution (for PGAH as for PGAV), which mirrors the conclusion of Wartman et al. (2013) for the 2011 Mw=9.0 Tohoku earthquake. However, the correction with the ratio of PGAH to PGAV appears to be stronger. Scatter plots of LC against PGAH/PGAV suggest that most of landslides are triggered for values that are bounded between PGAH/PGAV values of 0.45 and 0.60 (Figure 7a). This area coincides exactly with the Principal Cordillera, corresponding to high mountains with a strong relief and steep slopes. The distribution is controlled by disrupted landslides (Figure 7c). For the coherent slides, the PGAH/PGAV band is very narrow, approximately 0.5 and 0.52 (Figure 7b). A secondary peak is observed in the range of 0.6 and 0.7. A much broader band for flows and lateral spreads is observed between 0.45 and 0.58 (Figure 7d).
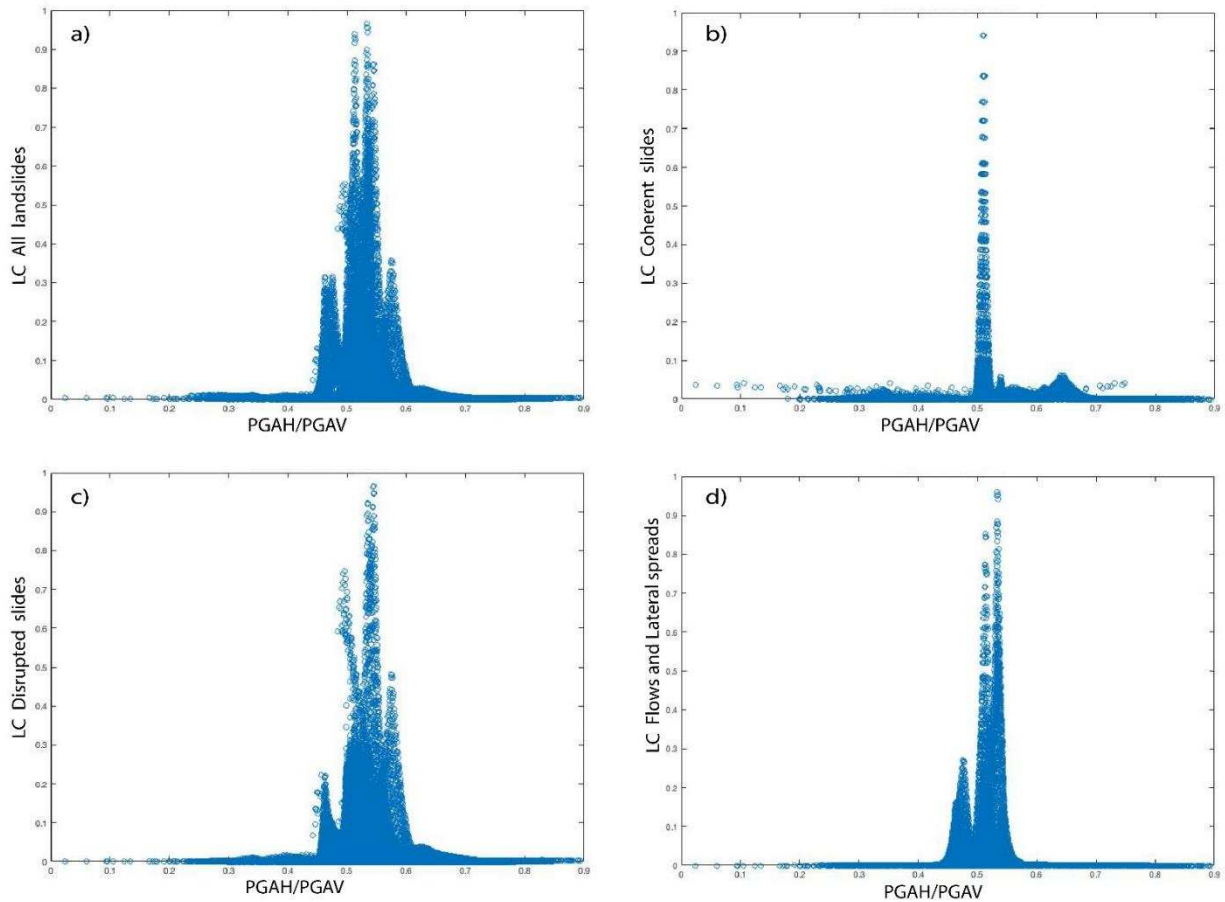

Figure 7. Scatter plots of landslide concentration (LC), obtained from Figure 6, vs PGAH/PGAV values obtained from map (Figure 3). 7a) Corresponds to all Landslide; 7b) disrupted landslide; 7c) coherent landslides; and 7d) flows and lateral spreads.

We also evaluated the potential correlation between LC parameter with distance by calculating the landslide smallest distance (linear distance) to the rupture plane, analogous to the analysis of Keefer (2000) for the 1989 Loma Prieta, California event (plotted in bins on numbers of landslides in Figure 8 and as a scattergraph of LC in Figure 8b). The rupture plane grid points were obtained by joint inversion from Lorito et al. (2011), and the smallest distance was calculated using a Matlab script developed by Escobar (2013).

Overall, a substantial number of landslides occur near the source, at distances from 20 to 40 km. This pattern reduces at 40 to 70 km. At 80 km from the source, landslide occurrence drastically increases and then starts to reduce systematically. A likely interpretation to the result could be related to the fact that rupture plane (zone) is parallel to the mountain ranges. Basins with low relative relief (i.e. low landslide

potential) located between the cordilleras typically lie at 40 to 60 km from the rupture plane. Therefore, landslide occurrence is not to be correlated directly to the distance to the rupture plane, but is mainly controlled by the surface relief.
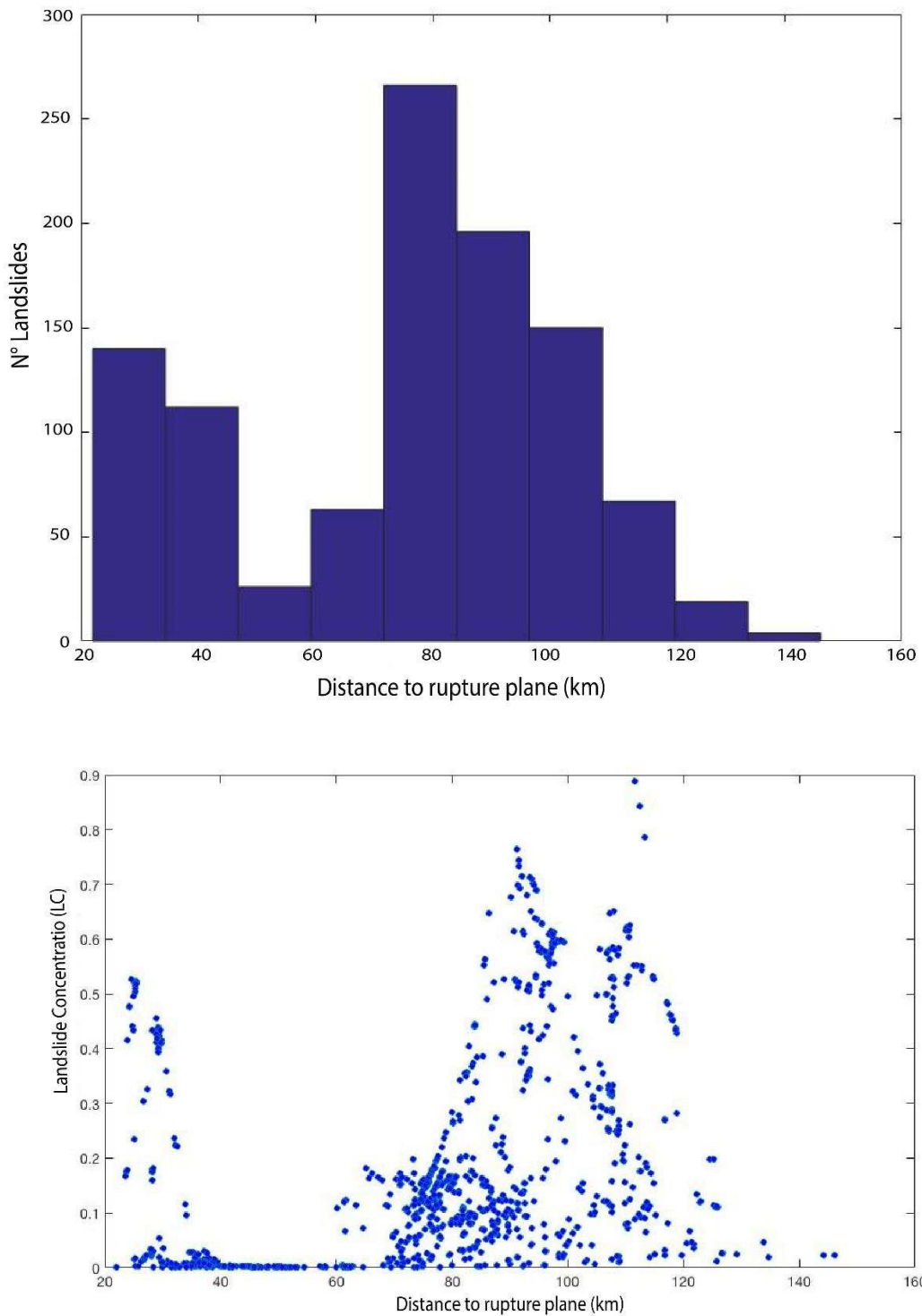

Figure 8. a) N° landslides vs distance to rupture plane. b) LC vs Distance to rupture plane

DISCUSSION

In general, there is a strong coincidence between the results of this study and those from a study of the 2010 M=9.0 Tohoku earthquake (Wartman et al. 2013), as follows:

- Given the width of the rupture zone generating this large magnitude earthquake, a substantial majority of landslides occurred in a zone underlain by the causative thrust.
- The spatial distribution of landslides is extremely heterogeneous, with clusters of landslides being observed.
- Disrupted landslides were the dominant type of landslides triggered by the Maule earthquake and associated aftershocks.
- A majority of landslides occurred in the youngest geologic units. The young rock materials are poorly cemented weak rocks and the degree of cementation of these poor quality rock masses is likely to be a controlling factor rather than the age.
- There is no clear correlation between ground motion (PGA) and landslide intensity. It should be recognized that PGA does not represent other potentially important characteristics such as frequency content, duration, or the multiple phases of shaking recorded at some locations, whose influence on landslides should be studied in more depth.

Figure 9 shows the relationship between the total number of landslide (N_{LT}) and earthquake moment magnitude (M_W) for shallow crustal and megathrust earthquakes (Table 2 of supplementary data (S1)). It is notable that the total number of landslides triggered for the megathrust earthquakes is substantially lower, typically by one to two orders of magnitude, than it would be expected for shallow crustal earthquakes. We suggest that there may be a fundamentally different landslide response to megathrust earthquakes in subduction plate contacts compared with shallow crustal events. The former tend to trigger a much smaller number of landslides compared to those generated by shallow crustal earthquakes.

Attenuation models predict PGA values, but not the specific waves that cause them (P, S or Surface waves). Earthquakes that generate fault rupture at the surface, are likely to produce greater amounts of surface waves, which typically is what causes damage. We can speculate that a megathrust earthquake suffers much higher surface waves attenuation than shallow crustal earthquakes, triggering a smaller amount of landslides.
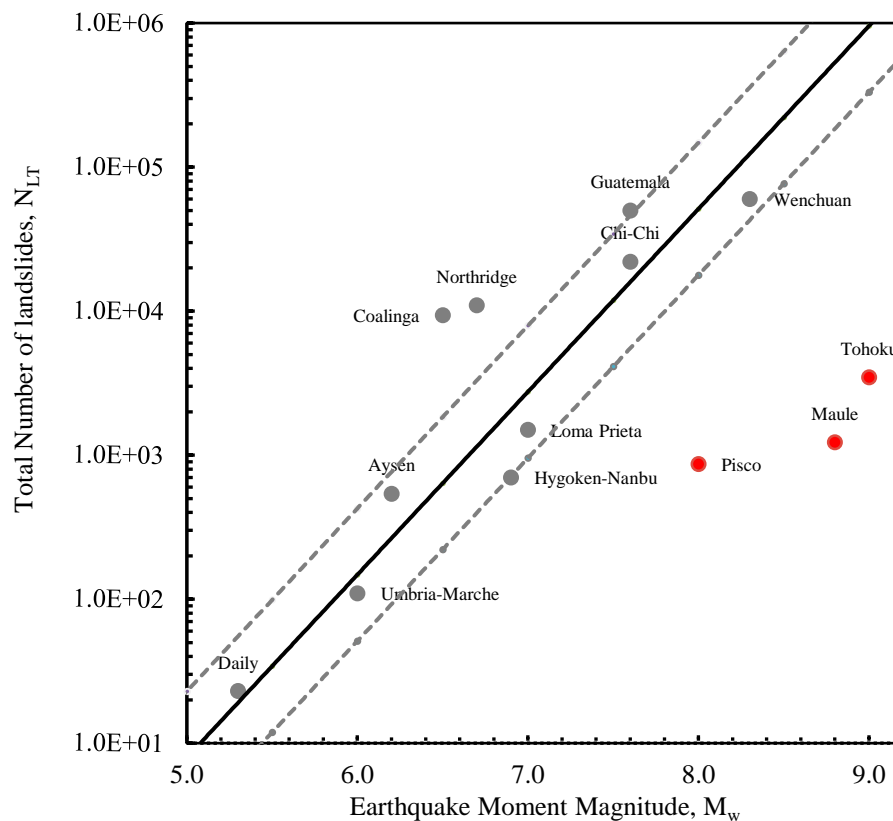
Figure 9. Dependence of Total number of landslide N_{LT} and earthquake moment magnitude M_W to shallow crustal (grey) and megathrust (red) earthquakes. Solid line is the correlation from the relationship proposed by Malamud et al. (2004b) with the grey dashed lines providing the corresponding error bounds. Data for the 13 earthquakes are given in Table 2 of supplementary material (S1).

It is difficult to draw definitive conclusions about this observation, given the limited number of megathrust events. However, we can speculate as to possible reasons for this effect. These might include:

1. In the case of the subduction zone earthquakes, the distance from the fault plane to the topography is much larger than is the case for many shallow crustal earthquakes. This may affect the key seismic parameters that control slope stability. Whilst it is conventionally considered that this parameter may be PGAH, this study and others fail to find a strong relationship between landslide occurrence and the regional distribution of PGAH. It is not known if this is because modelled values of PGAH are incorrect, or that this parameter is not the key control.

2. The type of faulting mechanism may affect the characteristics of the seismic waves, such as for example the frequency range. Whether faulting produces surface rupture may also change the characteristics of shaking.

3. The availability of topography susceptible to failure varies between the two settings, with shallow crustal earthquakes often being associated with areas of steep terrain and high relative relief close to the fault plane. Whilst megathrust earthquake may also be associated with areas of steep terrain, these are typically at a much larger distance from the fault plane.

4. The susceptibility of the rocks may vary across the two tectonic settings. Thus, for example, the lithologies close to the fault plane for shallow crustal earthquakes may be weaker, with higher densities of persistent discontinuities, allowing more landslides to be generated

In the case of the 2011 Mw=9.0 Tohoku earthquake, the majority of the disrupted landslides appear to have originated at or near the crest of steep slope, suggesting that the topographic modification of ground motion played a role in their initiation (Warman et al. 2013). Topographic amplification is a site effect caused by the interaction of the incoming seismic waves with certain geomorphological features, such as steep slopes in areas of strong topographic relief, which results in larger amplitudes of the ground motion toward the ridge crests (e.g., Densmore and Hovius 2000, Sepúlveda et al. 2005, Meunier et al. 2008). Meunier et al. (2008) proposed a graphic method to represent the position of landslides on the slopes, combining the normalized distance of the landslide top to the ridge crest and the normalized distance of the landslide toe to the nearest stream. This method is applied in Figure 10. A concentration of circles close to the y-axis represents that coseismic landslides are strongly clustered near ridge crests, such as for shallow crustal earthquakes of Northridge (Meunier et al. 2008) and Aysén in southern Chile (Sepúlveda et al. 2010). In the last one, about two thirds of the landslides start in the upper quarter of the slope, while over 90% start in the upper half, which suggests that larger ground motions due to topographic site effects influenced the triggering of landslides during the earthquake (Sepúlveda et al. 2010). Figure 10 shows that landslides induced by the Maule earthquake are not clustered close to the ridge tops, so we could disregard a predominant topographic site effect in their generation, although it may have played a role locally.
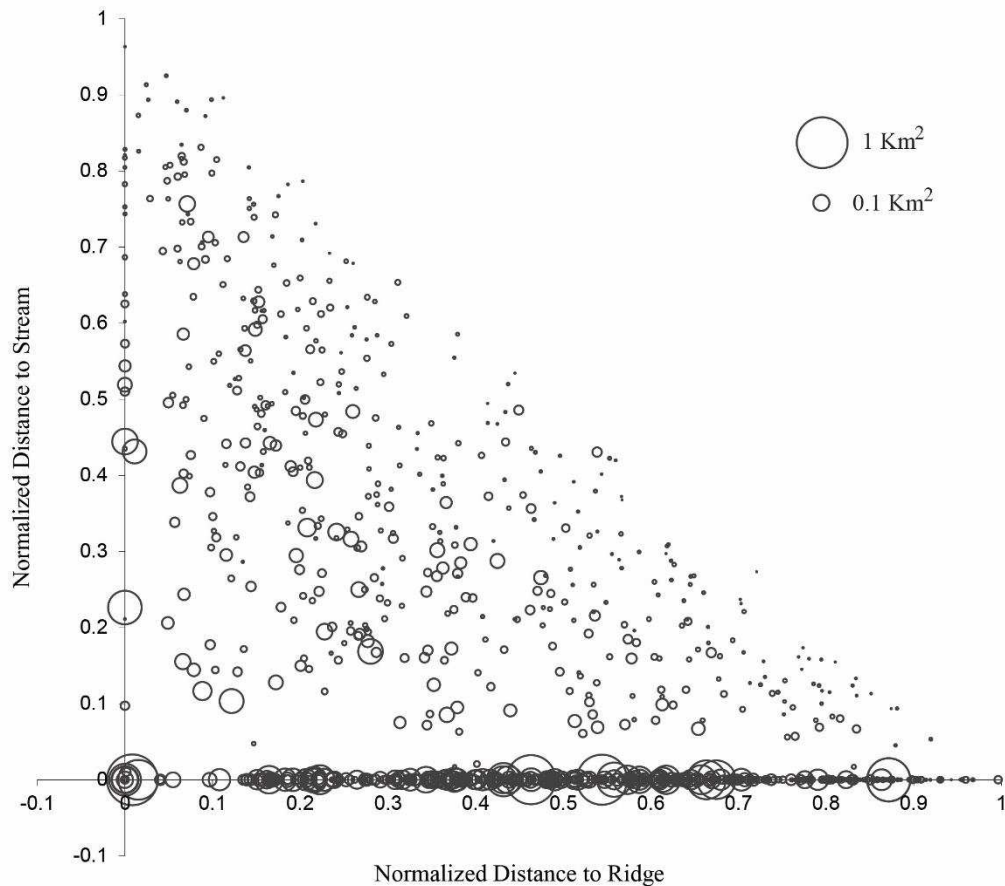
Figure 10. Landslide relative position on the slopes. Normalized distance of the landslide crowns to ridge tops against normalized distance of landslide toes to nearest streams. The size (surface area) of the landslide is indicated with a circle of variable diameter.

It is difficult to establish a direct correlation between observed PGA values and does PGA´s obtained from ground motion prediction equations. In this context, GMPE for Chilean subduction zone (Idini et al. 2017), estimate a decrease from c. 0.2g to 0.15g (in a normalized logarithmic scale) up to a rupture distance c. 200 km. These results correlate well with our PGAV map (Figure 5b) but not with PGAH values (Figure 5a) that could be caused by other effects (e.g. site effect, Angol station).

We observe that the key seismic parameter that appears to explain the distribution of landslides best is the ration between PGAH and PGAV. It is not clear as to why this might be the case, but Brain et al. (2014) suggested that wave phasing, and the associated coincidence of horizontal and vertical accelerations, may play a key role in determining slope response. The role of slip surface normal accelerations in the initiation of landslides is seen as significant by Huang et al. (2001) and the complexity generated by rapidly fluctuating normal and shearing stresses during shaking deserves much further investigation.

CONCLUSIONS

We have compiled and analysed an inventory of landslides triggered by the 2010 M=8.8 Maule earthquake in the Chilean subduction zone. We find that the number and density of landslides triggered by the earthquake is lower than might have been expected for a seismic event of this scale (by one to two orders of magnitude) than for a shallow crustal earthquake of a similar or even lower magnitude, in common with observations for the 2011 Mw=9.0 Tohoku earthquake in Japan. Landslides occurred primary on low to moderate angled slopes towards the western side of the main Andean range, accompanied by clusters of landslides in the lower Coastal Range. For the 2010 Maule earthquake, we

suggest that relief exerted a strongly dominant control on coseismic landsliding, with lithology the second most relevant conditioning factor, with more landslides in younger rocks. We find a poor correlation between PGA and landslide occurrence, and with distance from the fault plane, but note a much stronger correlation between landslide concentration and the ratio between horizontal and vertical peak accelerations.

These results suggest that the number and distribution of coseismic landslides may differ significantly between megathrust and shallow crustal earthquakes, although further research through the collation of high quality inventories is required as further megathrust earthquakes occur. At present the paucity of inventories for megathrust earthquakes defies the proposal of a definitive explanation for this observation. However, it may prove to be important in terms of the relative distribution of hazards associated with earthquakes in areas affected by megathrust earthquakes. Chile has a high concentration of large magnitude rock avalanches in the Andes; these results may suggest that they may be associated with proximal, lower magnitude shallow crustal earthquakes rather than larger but distal megathrust events.

REFERENCE

Angermann D, Klotz J, Reigber C (1999) Space-geodetic estimation of the Nazca-South America Euler vector. Earth and Planetary Science Letters 171: 329-334

Allmendinger RW, Jordan TE, Kay SM, Isacks BL (1997) The evolution of the Altiplano-Puna plateau of the Central Andes. Annual review of earth and planetary sciences 25(1):139-174

Astroza M, Ruiz S, Astroza R (2012) Damage assessment and seismic intensity analysis of the 2010 (Mw 8.8) Maule earthquake. Earthquake Spectra 28(S1):S145-S164

Barrientos SE (2010) Terremoto (M= 8.8) del 27 de febrero de 2010 en Chile. Revista de la asociación Geológica Argentina 67(3): 412-420

Bird P (2003) An updated digital model of plate boundaries. Geochem.Geophys.Geosyst. 4(1):1027

Boroschek R, Contreras V, Kwak DY, Stewart JP (2012) Strong ground motion attributes of the 2010 Mw 8.8 Maule, Chile, earthquake. Earthquake Spectra 28(S1):S19-S38

Brain MJ, Rosser NJ, Norman EC, Petley DN (2014) Are microseismic ground displacements a significant geomorphic agent?. Geomorphology (207):161-173

Campos J, Hatzfeld D, Madariaga R, Lopez G, Kausel E, Zollo A, Barrientos S, Lyon-Caen H (2002) The 1835 seismic gap in South Central Chile, Phys. Earth Planet. Int. 132:177–195

Cisternas A (2011) El país más sísmico del mundo. Revista Anales Séptima Serie

Charrier R, Ramos VA, Tapia F, Sagripanti L (2015) Tectono-stratigraphic evolution of the Andean Orogen between 31 and 37°S (Chile and Western Argentina). Geological Society Special Publications, London, pp 13-61

Dai FC, Xu C, Yao X, Xu L, Tu XB, Gong QM (2011) Spatial distribution of landslides triggered by the 2008 Ms 8.0 Wenchuan earthquake. China Journal of Asian Earth Sciences 40(4):883-895

Delouis B, Nocquet JM, Vallée M (2010) Slip distribution of the February 27, 2010 Mw = 8.8 Maule earthquake, central Chile, from static and high-rate GPS, InSAR, and Broadband teleseismic data. Geophysical Research Letters https://doi:10.1029/ 2010GL043899

Densmore A, Hovius N (2000) Topographic fingerprints of bedrock landslides. Geology 28(4):371–374

Escobar P, (2013) Inventario de remociones en masa desencadenadas por el sismo del 27 de febrero de 2010 en Chile central. Memoria de título, Universidad de Chile, Departamento de Geología

Gorum T, Fan X, van Westen CJ, Huang RQ, Xu Q, Tang C, Wang G (2011) Distribution pattern of earthquake-induced landslides triggered by the 12 May 2008 Wenchuan Earthquake. Geomorphology. doi:10.1016/j.geomorph.2010.12.030.

Havenith HB, Torgoev A, Braun A, Schlögel R, Micu M (2016) A new classification of earthquake-induced landslide event sizes based on seismotectonic, topographic, climatic and geologic factors. Geoenvironmental Disasters 3(1):6

Huang CC, Lee YH, Liu HP, Keefer DK, Jibson RW (2001) Influence of Surface-Normal Ground Acceleration on the Initiation of the Jih-Feng-Erh-Shan Landslide during the 1999 Chi-Chi, Taiwan, Earthquake. Bulletin of the Seismological Society of America, 91(5):953–958

Hung and Ju-Jiang (2000) Chi-Chi Earthquake induced landslides in Taiwan. Earthquake Engineering and Engineering Seismology 2(2):25-33

Idini, B, Rojas F, Ruiz S, Pastén C (2017) Ground motion prediction equations for the Chilean subduction zone. Bulletin of Earthquake Engineering, 15(5):1853-1880

Isacks BL (1988) Uplift of the central Andean plateau and bending of the Bolivian orocline. Journal of Geophysical Research: Solid Earth 93(B4):3211-3231

Jibson RW, Harp EL, Schulz W, Keefer DF (2006) Large rock avalanches triggered by the M 7.9 Denali Fault, Alaska, earthquake of 3 November 2002. Engineering Geology 83:144-160

Jibson E (1995) Inventory of landslides triggered by the 1994 Northridge, California earthquake. http://pubs.usgs.gov/of/1995/ofr-95-0213/

Jordan TE, Isacks B, Allmendinger R, Brewer J, Ramos V, Ando C (1983) Andean tectonics related to geometry of the subducted Nazca plate. Geol. Soc. Am. Bull 94:341-361

Kamp U, Growley BJ, Khattak GA, Owen LA (2008) GIS-based landslide susceptibility mapping for the 2005 Kashmir earthquake region. Geomorphology 101(4):631-642

Keefer DK (2002) Investigating Landslides Caused By Earthquakes – a Historical Review. Surveys in geophysics (1):473–510

Keefer DK (2000) Statistical analysis of an earthquake-induced landslide distribution—the 1989 Loma Prieta, California event. Engineering geology 58(3):231-249

Keefer, DK (1984) Landslides caused by earthquakes. Geological Society of America Bulletin 95:406-421

Lacroix P, Zavala B, Berthier E, & Audin L (2013) Supervised method of landslide inventory using panchromatic SPOT5 images and application to the earthquake-triggered landslides of Pisco (Peru, 2007, Mw8. 0). Remote Sensing 5(6):2590-2616

Larsen IJ, Montgomery DR, Korup O (2010) Landslide erosion controlled by hillslope material. Nature Geoscience 3(4):247

Lay T, Ammon CJ, Kanamori H, Koper KD, Sufri O, Hutko AR (2010) Teleseismic inversion for rupture process of the 27 February 2010 Chile (Mw 8.8) earthquake. Geophysical Research Letters https://doi.org/10.1029/2010GL043379

Lorito S, Romano F, Atzori F, Tong X, Avallone A, McCloskey J, Cocco M, Boshi E, Piatanesi A, (2011) Limited overlap between the seismic gap and co-seismic slip of the great 2010 Chilean earthquake, Nature Geoscience Letters Nature Geoscience, 4(3):173

Malamud BD, Turcotte DL, Guzzetti F, Reichenbach P (2004a) Landslide inventories and their statistical properties. Earth Surface Processes and Landforms 29(6):687-711

Malamud BD, Turcotte DL, Guzzetti F, Reichenbach, P (2004b) Landslides, earthquakes, and erosion. Earth and Planetary Science Letters 229(1-2):45-59

Marc O, Hovius N, Meunier P, Gorum T, Uchida T (2016) A seismologically consistent expression for the total area and volume of earthquake-triggered landsliding. Journal of Geophysical Research: Earth Surface, 121(4), 640-663

Mardones M, Rojas J (2012) Procesos de remoción en masa inducidos por el terremoto del 27F de 2010 en la franja costera de la Región del Biobío, Chile. Revista de Geografía Norte Grande 53:57-74

Meunier P, Hovius N, Haines JA (2008) Topographic site effects and the location of earthquake induced landslides. Earth and Planetary Science Letters (275):221-232

Moreno M, Klotz J, Melnick D, Echtler H, Bataille K (2008) Active faulting and heterogeneous deformation across a megathrust segment boundary from GPS data, south central Chile (36-39 S). Geochemistry Geophysics Geosystems, 9 12:Q12024

Moya S, Sepúlveda SA, Serey A, García M (2015) Remociones en masa generadas por el terremoto del Maule del 2010 en la Península de Arauco. In XIV Congreso Geológico de Chile Actas, La Serena

Moya S (2016) Comportamiento monotónico y cíclico de suelos y rocas blandas afectadas por remociones en masa cosísmicas. Universidad de Chile, Departamento de Geología

Owen LA, Kamp U, Khattak GA, Harp EL, Keefer DK, Bauer MA (2008) Landslides triggered by the 8 October 2005 Kashmir earthquake. Geomorphology 94(1):1-9

Pankhurst R, Hervé F (2007) Introduction and overview. The Geological Society of London, pp 1-4.

Pardo-Casas F, & Molnar P (1987) Relative motion of the Nazca (Farallon) and South American plates since Late Cretaceous time. Tectonics 6(3):233-248

Qi S, Xu Q, Lan H, Zhang B, Liu J (2010) Spatial distribution analysis of landslides triggered by 2008.5.12 Wenchuan Earthquake, China Engineering Geology 116 (1–2):95-108

Rodriguez CE and Bommer JJ, Chandler RJ (1999) Earthquake-induced landslides: 1980-1997. Soil Dynamics and Earthquake Engineering 18:325-346

Ruegg, JC, Rudloff A, Vigny C, Madariaga R, De Chabalier JB, Campos J, Kausel E, Barrientos S, Dimitrov D (2009) Interseismic strain accumulation measured by GPS in the seismic gap between Constitución and Concepción in Chile. Physics of the Earth and Planetary Interiors 175:78-85

Ruiz S, Madariaga R, Astroza M, Saragoni R, Lancieri M, Vigny C, Campose J (2012) Short-Period Rupture Process of the 2010 Mw 8.8 Maule Earthquake in Chile. Earthquake Spectra 28 (S1):S1–S18

Saragoni R, y Ruiz S (2012) Implicancias y nuevos desafíos del diseño sísmico de los acelerógramas del Terremoto del 2010, en Mw=8.8: Terremoto en Chile, 27 de febrero 2010. Primera edn, Departamento Ingeniería Civil FCFM Universidad de Chile, pp 127-146

Sato H, Hasegawa H, Fujiwara S, Tobita M, Koarai M, Une H, Iwahashi J (2007) Interpretation of landslide distribution triggered by the 2005 Northern Pakistan earthquake using SPOT 5 imagery. Landlsides 4:113-122

Sheffels BM (1990) Lower bound on the amount of crustal shortening, in the central Bolivian Andes. Geology 18(9):812-815

Sepúlveda SA, Murphy W, Petley DN (2005) Topographic controls on coseismic rock slides during the 1999 Chi-Chi Earthquake, Taiwan. Quarterly Journal of Engineering Geology and Hydrogeology 38:189-196

Sepúlveda SA, Serey A, Lara M, Pavez A, Rebolledo S (2010) Landslides induced by the 2007 Aysen Fjord earthquake, Chilean Patagonia. Landslides 7(4):483-492

Serey A, Escobar P, Moya S, Sepúlveda SA, Petley D (2017) Landslide inventory of the 2010 Mw 8.8 Maule earthquake, Central Chile. 16th World Conference on Earthquake 16WCEE 2017: 1873

SERNAGEOMIN (2003) Mapa Geológico de Chile a escala 1:1.000.000: versión digital. Servicio Nacional de Geología y Minería, Publicación Geológica Digital N°4

Soeters R Van Western CJ (1996) Slope Instability Recognition, Analysis and Zonation. In: Turner, A.K. and Schuster, R.L. (eds). Landslides, investigation and mitigation. Transportation Research Board, National Research Council, Special Report 247, National Academy Press, Washington D.C., U.S.A., 129-177

Terzaghi K (1950) Mechanisms of landslides, Application of Geology to Engineering Practice. Berkey Volume S Geological Soc. of America

Tong X, Sandwell D, Luttrell K, Brooks B, Bevis M, Shimada M, Foster J, Smalley R, Parra H, Baez JC, Blanco M, Kendrick E, Genrich J, Caccamise D (2010) The 2010 Maule, Chile earthquake: Downdip rupture limit revealed by space geodesy. Geophysical Research Letters, 37 (24): L24311

Verdugo R, González J, González V, Torres A (2012) Características y efectos del fenómeno de licuefacción. En Mw=8.8: Terremoto en Chile, 27 de febrero 2010. Primera edn., Departamento Ingeniería Civil FCFM Universidad de Chile

Wartman J, Dunham L, Tiwari B, Pradel D (2013) Landslides in Eastern Honshu induced by the 2011 off the Pacific Coast of Tohoku earthquake. Bulletin of the Seismological Society of America 103 (2B):1503–1521

Wessel P, and Smith WHF (1998) New, improved version of the Generic Mapping Tools released. Eos, Transactions American Geophysical Union, 79(47): 579-579

SUPPLEMENTARY MATERIAL (S1)

Landslide volume methodology

We used published area-volume relationships, $V'=\lambda A'^\gamma$ (Larsen et al., 2010), to estimate the volume of a landslide, V', from its mapped disturbed area, A'. It was assumed that disrupted landslides with $A' > 10^5$ m^2 involved bedrock and that smaller disrupted landslides were mixed bedrock and soil failures. Our landslide maps do not distinguish between scar and deposit, lumping the two in one area measure. To calculate volume is necessary scar area. Thus, we have applied a blanket correction to reduce the total area of a landslide to its scar area and obtained a conservative volume estimate. According to Larsen et al. (2010), scars and deposits have area-volume relations with the same power law exponent, implying constant size ratios between scar and deposit areas of 1.1 and 1.9 for mixed and bedrock landslides, respectively. Hence, we estimated the scar area by dividing the mapped landslide area by 2.1 and 2.9 for mixed soil and bedrock and solely bedrock landslides, respectively, assuming that runout distance was equal to the scar length.

Table 1. Data obtained from the Accelerograph Chilean Network, Universidad de Chile. Peak horizontal ground acceleration (PGAH), peak vertical ground acceleration (PGAV), peak horizontal ground velocity (PGVH), peak vertical ground velocity (PGVV).

Seismological station	PGAH	PGAV	PGVH	PGVV	Latitude	Longitude
Copiapó	0.029	0.008	0.0300	0.010	-27.3737	-70.3216
Vallenar	0.019	0.010	0.0275	0.015	-28.5766	-70.7552
Papudo	0.421	0.155	0.1670	0.248	-32.5200	-71.4500
Viña del mar centro	0.034	0.186	0.3260	0.124	-33.0249	-71.5529
Viña del mar el sato cerro	0.353	0.260	0.3760	0.422	-33.0472	-71.5099
Valparaiso UTSFM	0.304	0.079	0.0780	0.082	-33.0300	-71.6200
Valparaiso almendral	0.265	0.145	0.2910	0.223	-33.0300	-71.6200
Llolleo	0.564	0.702	0.2350	0.304	-33.6200	-71.6000
Santiago centro	0.310	0.182	0.1680	0.186	-33.4670	-70.6520
Santiago Maipu	0.562	0.240	0.4400	0.220	-33.5087	-70.7714
Santiago La FLorida	0.236	0.130	0.1500	0.105	-33.5139	-70.6052
Santiago Peñalolén	0.295	0.280	0.2930	0.127	-33.5014	-70.5792
Santiago Puente Alto	0.265	0.130	0.3145	0.162	-33.5780	-70.5810
Matanzas	0.461	0.234	0.3700	0.277	-33.9600	-71.8700
Hualañe	0.461	0.390	0.3880	0.350	-34.9763	-71.8059
Talca	0.477	0.243	0.1950	0.274	-35.4300	-71.6300
Constitución	0.640	0.352	0.4100	0.620	-35.3400	-72.4000
Concepción	0.402	0.397	0.5800	0.492	-36.8283	-73.0482
Angol	0.928	0.281	0.3600	0.087	-37.7900	-72.7100
Valdivia	0.138	0.051	0.1840	0.066	-39.8314	-73.2391
Curicó	0.471	0.198	0.2770	0.294	-34.9905	-71.2367
Concepción San Pedro	0.650	0.550	No data	No data	-36.8442	-73.1086
Santiago Antumapu	0.340	0.210	No data	No data	-33.5692	-70.6335
El Roble	0.190	0.110	No data	No data	-32.9763	-71.0149
Pichilemu	0.160	0.130	No data	No data	-34.3904	-72.0034
Santiago San Jose de Maipo	0.470	0.240	No data	No data	-33.8475	-70.2035
Santiago FCFM	0.170	0.140	No data	No data	-33.4563	-70.6624
Casablanca	0.330	0.230	No data	No data	-33.2590	-71.1376
Los Molles	0.160	0.070	No data	No data	-32.2320	-71.5070
Santiago Las Americas	0.310	0.160	No data	No data	-33.4520	-70.5310
Olmué	0.360	0.150	No data	No data	-32.9940	-71.1730
Viña del mar Marga Marga	0.340	0.260	No data	No data	-33.0470	-71.5100
Los Vilos	0.030	0.020	No data	No data	-31.9200	-71.5000
Zapallar	0.180	0.110	No data	No data	-32.5700	-71.4700
Santiago Santa Lucia	0.320	0.260	No data	No data	-33.4400	-70.6400

| Cabildo | 0.320 | 0.130 | No data | No data | -32.4270 | -71.0690 |
| Melipilla | 0.770 | 0.380 | No data | No data | -33.6800 | -71.2200 |

Table 2. Comparative table of different landslide-generating earthquakes

Earthquake	Mw	Earthquake type	N_{LT}	m_L
Daily City, CA, USA	5.3**	shallow crustal	23 [a]	1.4
Umbria-Marche, Italy	6.0	shallow crustal	110 [a]	2.0
Aysén, Chile	6.2	shallow crustal	538 [b]	2.7
Coalinga, CA, USA	6.5	shallow crustal	9,389 [a]	4.0
Northridge, CA, USA	6.7	shallow crustal	11,000 [c]	4-0
Hygoken-Nanbu, Japan	6.9	shallow crustal	700 [a]	2.8
Loma Prieta, CA, USA	7.0	shallow crustal	1,500 [a]	3.2
Chi-chi, Taiwan	7.6	shallow crustal	22,000 [d]	4.3
Guatemala	7.6	shallow crustal	50,000 [a]	4.7
Wenchuan, China	8.3	shallow crustal	60,000 [e]	4.8
Pisco, Perú	8.0	megathrust	866 [f]	2.9
Maule, Chile	8.8	megathrust	1,226 [d]	3.1
Tohoku, Japan	9.0	megathrust	3,477 [e]	3.5

*N_{LT} is the total number of landslides associated with the triggered event; *m_L is the landslide-event magnitude ($m_L = \log N_{LT}$; Malamud et. al 2004b); **Earthquake magnitudes are all moment or equivalent moment magnitudes except for Daily City (local magnitude); [a] Keefer (2002); [b] Sepúlveda et al. (2010); [c] Jibson (1995); [d] Hung and Ju-Jiang (2000); [e] Gorum et al., 2011; [f] Lacroix et al. (2013) ; [g] This study; [h] Wartman et al. (2013)
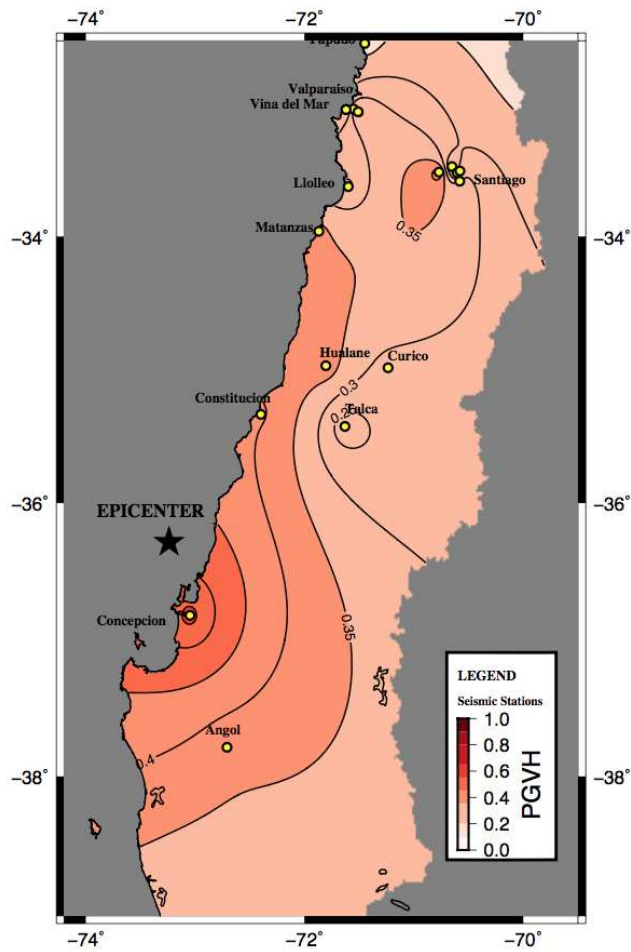
Figure 1. Interpolated maps of the peak ground accelerations of PGVH.

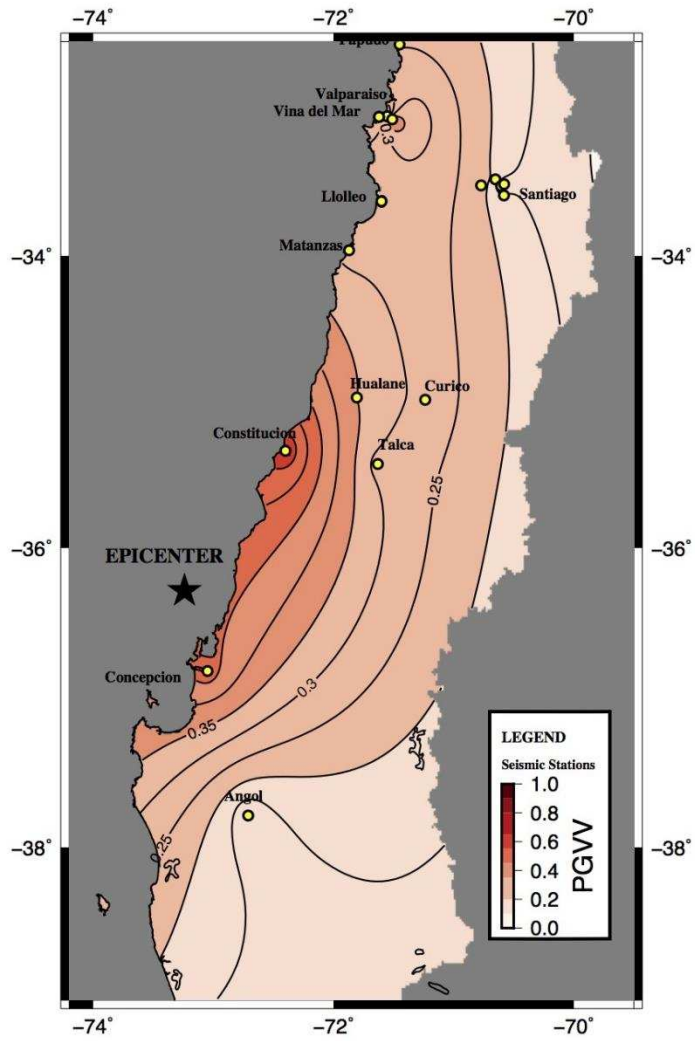**Figure 2.** Interpolated maps of the peak ground accelerations of PGVV.
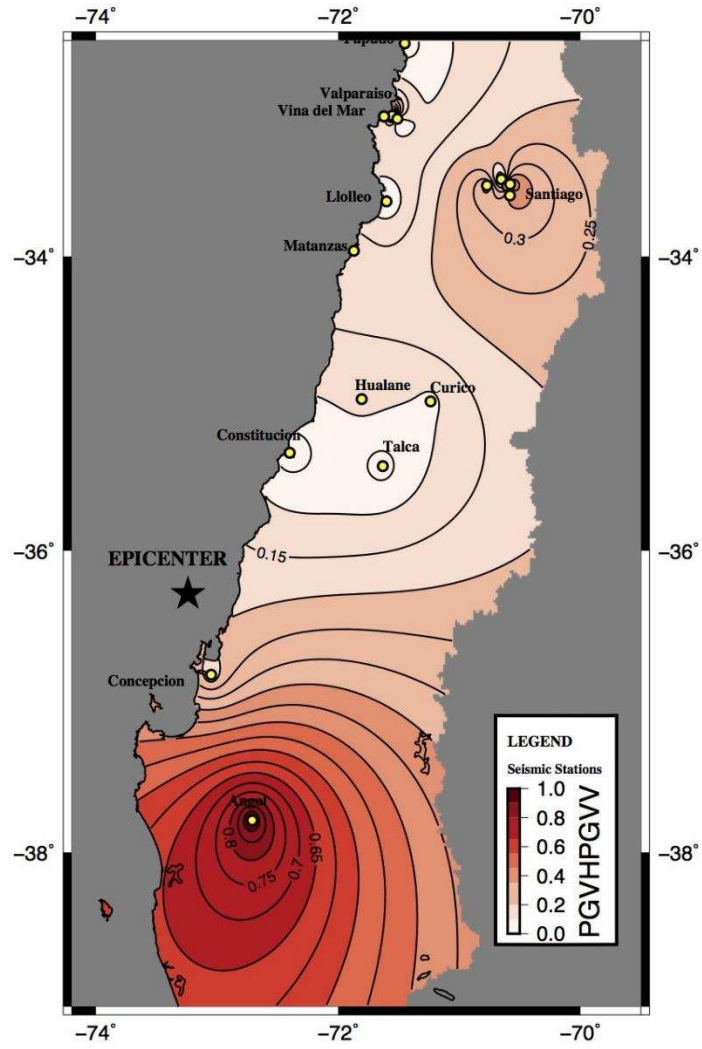
Figure 3. Interpolated maps of the peak ground accelerations of PGVH/PGVV.